arXiv:1111.3476v1 [cond-mat.str-el] 15 Nov 2011

BaVS$_3$ probed by V L edge X-ray absorption spectroscopy

V. Ilakovac[1,2,*], N. B. Brookes[3], J. Criginski Cezar[3], P. Thakur[3], V. Bisogni[3], C. Dallera[4],
G. Ghiringhelli[4], L. Braicovich[4], S. Bernu[5], H. Berger[6], L. Forró[6], A. Akrap[6], C. F. Hague[1*]
[1]*Université Pierre et Marie Curie, CNRS UMR 7614, LCP-MR, F-75231 Paris, France*
[2]*Université de Cergy-Pontoise, F-95031 Cergy-Pontoise, France*
[3]*ESRF, B.P. 220, 38043 Grenoble Cedex, France*
[4]*Politecnico di Milano, Piazza Leonardo da Vinci 32, 20133 Milano, Italy*
[5]*Laboratoire de Physique de Solides, CNRS-UMR 8502,*
Université Paris-Sud, Batiment 510, 91405 Orsay Cedex, France
[6]*Ecole Polytechnique Federale de Lausanne CH-1015, Switzerland*
(Dated: November 16, 2011)

Polarization dependent vanadium L edge X-ray absorption spectra of BaVS$_3$ single crystals are measured in the four phases of the compound. The difference between signals with the polarization $\mathbf{E}\perp\mathbf{c}$ and $\mathbf{E}\|\mathbf{c}$ (linear dichroism) changes with temperature. Besides increasing intensity of one of the maxima, a new structure appears in the pre-edge region below the metal-insulator transition. More careful examination brings to light that the changes start already with pretransitional charge density wave fluctuations. Simple symmetry analysis suggests that the effect is related to rearrangements in E_g and A_{1g} states, and is compatible with the formation of four inequivalent V sites along the V-S chain.

PACS numbers: 78.40.-q, 71.30.+h, 71.27.+a, 71.45.Lr, 71.70.Ch, 71.45.-d

I. INTRODUCTION

Complex materials often display rich phase diagrams where different types of instabilities lead to unusual properties related to various ordering phenomena. Understanding the interplay between lattice, charge, spin and orbital degrees of freedom is one of most challenging aspects of correlated electron systems.

Barium vanadium sulfide, BaVS$_3$, is a particularly intriguing material because its structural, electrical and magnetic properties point to a combination of quasi-1D and 3D behavior. Its room temperature structure consists of hexagonal packing of quasi 1D-chains of face-sharing VS$_6$ octahedra directed along the **c** axis [1]. The ratio of inter-chain to intra-chain V-V distances being greater than 2, a high conductivity anisotropy ratio (σ_c/σ_a) can be expected. Surprisingly, σ_c/σ_a is only about three [2]. Lowering the temperature induces a zig-zag deformation of the V chains at $T_S = 240$ K and reduces the crystal symmetry from hexagonal to orthorhombic [1], but does not significantly change its conductive and magnetic properties. In both phases, it is a paramagnetic metal. Below $T_{MI} = 69$ K it becomes a paramagnetic insulator (PI). The metal-insulator (MI) transition is driven by a Peierls instability [3], accompanied by a change to a monoclinic structure [4]. At $T_N = 31$ K, it undergoes a third phase transition to the lowest temperature (ground) state which has an incommensurate antiferromagnetic (AF) order in the (**a**,**b**) plane [5]. Recent resonant magnetic x-ray scattering reveal additional incommensurability along the **c** axis in the AFI ground state, while the supporting time-dependent density functional theory simulations indicate that the spins lie within the (**a**,**b**) plane and are polarized along the monoclinic **a** axis [6].

Diffuse X-ray scattering experiments [3] have demonstrated that the MI transition is driven by a 1D instability of the electron gas. It leads to the formation of charge density waves (CDW) at the critical wave vector $\boldsymbol{q_c} = 2\boldsymbol{k_F}$, preceded by pretransitional fluctuations. But the physical properties of BaVS$_\mathbf{3}$ are not those of a standard quasi-1D system. First, the wave vector $\boldsymbol{q_c}$= 0.5 **c*** (**c*** stands for the reciprocal lattice vector related to **c**) indicates that only one of the two d electrons per unit cell (*uc*) participates directly in the CDW. On the other hand, instead of a typical Pauli behavior of a 1D electron gas in the metallic phase, it has a Curie-Weiss behavior with an effective magnetic moment of $\mu = 1.2\ \mu_B$ corresponding to approximately one localized spin per two vanadium sites [2]. All these properties point to an unusual situation with *one* electron per *uc* delocalized along the **c*** direction driving the CDW formation. The *other* is localized and responsible for the magnetic behavior.

Local density approximation (LDA) calculations indicate an interplay between two different types of electron states at the Fermi level: two narrow E_g bands, and one dispersive band with mainly A_{1g} character extending along the **c*** direction [7, 8]. But the LDA filling of the A_{1g} band is almost complete ($n_{A_{1g}} \approx 1.90$ per *uc*), which overestimates the itinerant character, and is incompatible with the above-mentioned experimental findings. Dynamical mean-field theory (DMFT) calculations show that strong enough charge correlation and exchange effects can bring $n_{A_{1g}}$ down to *one* per *uc* [9].

Both types of electron states, delocalized (charge degrees of freedom), and localized (magnetic properties), are modified at the MI transition. A charge gap of about

---

*Electronic address: vita.ilakovac-casses@upmc.fr

phase	AFI	mPI	oPM	hPM
T_c	T_N= 31 K	T_{MI}= 69 K	T_S= 240 K	
structure	monoclinic	monoclinic	orthorhombic	hexagonal
space group	Im	Im	$Cmc2_1$	$P6_3mmc$
point group	m (C_{1h})	m (C_{1h})	$mm2$ (C_{2v})	$\overline{3}m$ (D_{3d})
N_V ($N_{ineq.}$)	4 (4)	4 (4)	2 (1)	2 (1)
magnetism	AF	para	para	para
transport	insulator	insulator	metal	metal

TABLE I: Physical properties of $BaVS_3$ in its four phases: Anti-Ferromagnetic Insulator (AFI), monoclinic Paramagnetic Insulator (mPI), orthorhombic (oPM), and hexagonal (hPM) Paramagnetic Metal. T_c stands for critical temperature, and N_V ($N_{ineq.}$) the number of (inequivalent) V atoms per unit cell.

50 meV [2] and a spin gap of 10-20 meV [10] are opened at T_{MI}, even if the spin degrees of freedom quench only in the AFI phase. But the mechanism of their interplay is not yet completely understood.

We have explored four $BaVS_3$ phases in single crystals by polarization dependent x-ray absorption spectroscopy (XAS) at the V L edges. After describing the experimental means for obtaining very high resolution contamination-free data we present the results and then discuss how the polarization dependence of the XAS data provides new insight into the subtle electronic structure changes that take place across a temperature range that covers all the phases of $BaVS_3$.

II. EXPERIMENT

Single crystals of $BaVS_3$ were grown by the tellurium flux method [11]. Two samples from different batches were cleaved *in-situ* along a plane parallel to the **c**-axis. After the cleaving at a pressure of 10^{-9} mbar, they were transferred via a fast insertion lock to the analysis chamber at the base pressure of 4 x 10^{-10} mbar. The experiments were performed using the helical undulator Dragon beam line ID08 at the European Synchrotron Radiation Facility (ESRF). At the V L_3 edge ($\approx$ 514 eV) the resolution was $\approx$ 100 meV. The incident light was normal to the sample surface and linearly polarized either parallel to the sample **c**-axis, or perpendicular to it. We periodically checked for energy shifts coming from the monochromator. The stability of the photon energy is estimated to be better than 40 meV. The V L edge XAS signal was measured in the total electron yield mode using the drain current from the sample holder.

III. RESULTS

V $L_{2,3}$ XAS results for $BaVS_3$ at room temperature for the two polarizations of the incoming light, $\mathbf{E}\perp\mathbf{c}$ and $\mathbf{E}\|\mathbf{c}$ are presented in Fig. 1. The spectra are normalized so as to obtain the same difference in amplitude below the L_3 edge and at 534 eV. They are separated by the $2p$ spin orbit coupling, into L_3 ($h\nu$ = 512-519 eV) and L_2 ($h\nu$ = 519-528 eV) regions. The V L_3 and L_2 maxima are at 516.2 eV and 523.2 eV, respectively, i.e. 7 eV apart. Their overall shape is closer to the spectra of vanadium metal [12] than to the spectra of vanadium oxides that tend to be more structured (see for example VO_2 [13] or V_2O_3 [14]).

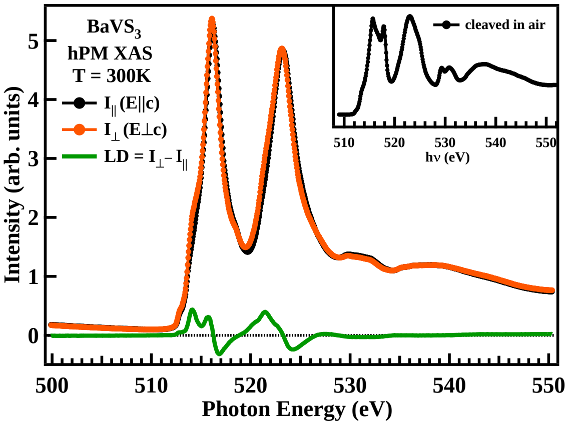

FIG. 1: (Color online) Paramagnetic Metallic phase (T = 300 K) XAS spectra of the *in-situ* cleaved sample for the two polarizations of the incoming light: $\mathbf{E}\perp\mathbf{c}$ (red dots) and $\mathbf{E}\|\mathbf{c}$ (black dots). The linear dichroism (LD = $I_{\perp}$-$I_{||}$) is also shown in the same graph (green line). The inset shows the spectra of a sample cleaved in air where the oxygen contamination is clearly visible above 530 eV. Extra features are observed at the V L_3 edge and the L_2 peak is broadened.

The O K XAS signal lies in the 530-545 eV region. By comparing with the inset in Fig. 1 it can be seen that the surface contamination is negligibly small. In particular the hump at 540 eV is very weak while the feature at 531 eV may even be intrinsic to the $BaVS_3$ spectrum. A similar feature is present in elemental vanadium, where it has been attributed to a van Hove singularity at the boundary of the V metal Brillouin zone [15]. The inset shows clearly that the oxygen contamination affects the V L edge. Additional structures show up at the high energy side of the V L_3 peak, and the V L_2 structure is broadened. In this sense, at least the surface of the slightly Ti-doped sample previously studied [16] was contaminated by oxygen.

The V $L_{2,3}$ maxima for the $\mathbf{E}\|\mathbf{c}$ polarization are at slightly higher photon energy than for the $\mathbf{E}\perp\mathbf{c}$ polarization. The shift is about 80 meV in the hPM phase. The peak position for V L_3 with $\mathbf{E}\perp\mathbf{c}$ excitation is 516.15 eV.

In order to show more clearly the polarization dependence of the XAS intensity, we subtracted $I_{||}$ ($\mathbf{E}\|\mathbf{c}$ spectra) from $I_{\perp}$ ($\mathbf{E}\perp\mathbf{c}$ spectra). This linear dichroism (LD) curve is presented in Fig. 1 for the hPM phase. The

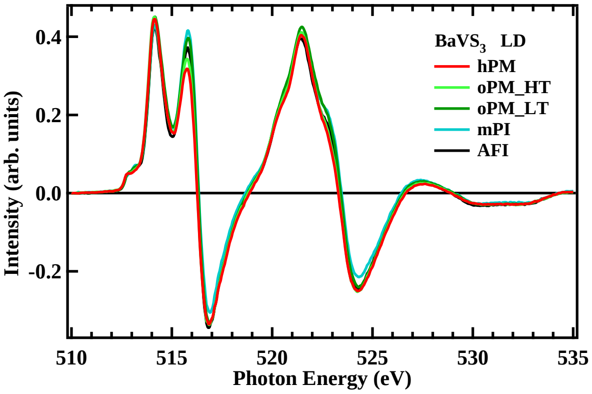

FIG. 2: (Color online) LD as a function of temperature. Red/light-green/dark-green/blue/black curves correspond respectively to the hPM/oPM-HT/oPM-LT/mPI/AFI temperature ranges.

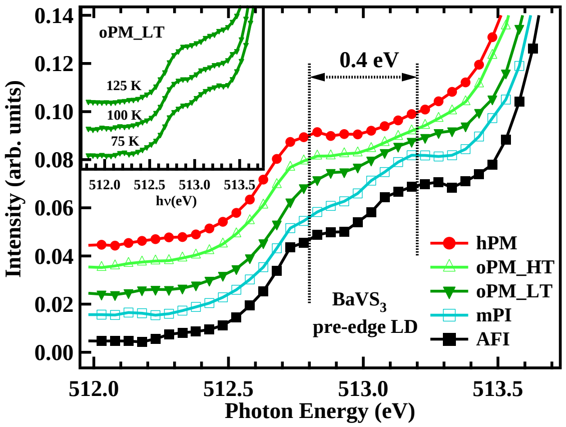

FIG. 3: (Color online) LD changes with temperature in the pre-edge region. The spectra are shifted vertically for clarity. Inset shows details of the temperature changes in the oPM-LT range.

change from positive to negative LD simply reflects the shift in the main XAS peak according to the polarization of the incident photons. This derivative-like shape hardly changes except for differences in amplitude as a function of the temperature or phase (Fig. 2).

When cooling to below $T_S = 240$ K (hPM to oPM), the shift increases to 110 meV. As a simplification we show the average spectrum taken at 300 K, 275 K and 250 K to represent the hPM phase, what we term the high temperature orthorhombic phase (oPM-HT) is taken as the average of spectra recorded at 225 K, 200 K, 175 K, and 150 K, and the low temperature orthorhombic phase (oPM-LT) spectrum is the average of data taken at 125 K, 100 K and 75 K. The mPI spectrum was recorded at 50 K and the AFI spectrum at 25 K. The shape of the main V L$_3$ XAS peak remains practically unchanged but the amplitude of the LD signal at 515.8 eV changes reflecting very small variations in the relative intensity of the $I_{||}$ and $I_{\perp}$ maxima. Another peak in the LD is observed at 514.2 eV, coinciding with the shoulder on the XAS data. Its amplitude is positive and remains practically unchanged across the range of measurements.

An essentially equivalent situation is observed for the L$_2$ edge. Here structures are not well resolved. This can be explained by the difference in lifetime broadening of the two edges, which is 0.78 eV (0.28 eV) for the V L$_2$ (L$_3$) [17].

A detailed examination of the low energy part of the spectra, brings to light structure at 512.8 eV. The LD data are shown in Fig. 3. As the temperature is lowered to the oPM-LT temperature range the intensity is increased at 513.2 eV, where a relatively strong extra peak is clearly present in both the mPI and AFI phases.

It should be underlined that we have observed the same low temperature behavior for *two* samples from different preparations. Fig. 4 shows the LD for the sample from the second batch demonstrating that the data are highly reproducible.

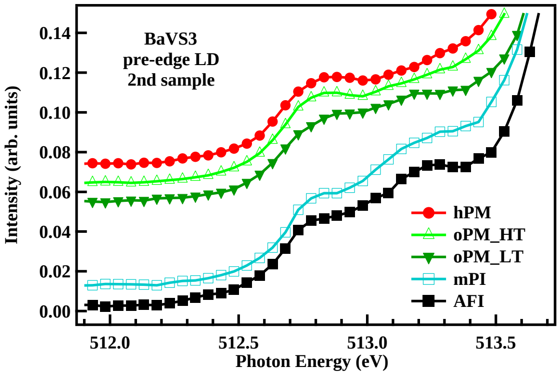

FIG. 4: (Color online) LD changes with temperature in the pre-edge region for the sample from another preparation is essentially the same.

IV. DISCUSSION

An elaborate theoretical interpretation of the BaVS$_3$ XAS spectrum is not presently available because of its structural complexity. We will therefore discuss our data in terms of a simplified analysis of orbital symmetries to help assess what information can be extracted from the XAS polarization dependence, along with our present knowledge of the physical properties of the material and the insight that can be gained from recent LDA-DMFT calculations [18].

First we need to calculate the polarization dependence of the $2p$ to $3d$ dipole transition in the material to assess the polarization effects.

Due to the inclination of the V-S octahedra in BaVS$_3$, it is convenient to present its V $3d$ states as a linear combination of cubic d orbitals (Eq. 1 and Fig. 5):

$$
\begin{aligned}
&A_{1g} = d_{z^2} \\
E_{g_1} &= -\sqrt{\frac{2}{3}}d_{x^2-y^2} + \sqrt{\frac{1}{3}}d_{yz} \\
E_{g_2} &= \sqrt{\frac{2}{3}}d_{xy} - \sqrt{\frac{1}{3}}d_{xz} \\
e_{g_1} &= \sqrt{\frac{1}{3}}d_{x^2-y^2} + \sqrt{\frac{2}{3}}d_{yz} \\
e_{g_2} &= \sqrt{\frac{1}{3}}d_{xy} + \sqrt{\frac{2}{3}}d_{xz},
\end{aligned}
\tag{1}
$$

The $2p \rightarrow 3d$ transition probabilities, according to dipolar selection rules, are given by

$$
P_d = \sum_{i=1}^{3} |\langle p_i|\mathbf{E}\cdot\mathbf{r}|d\rangle|^2 \tag{2}
$$

where p_i represents three V $2p$ orbitals and d can be any of the five V $3d$ orbitals: A_{1g}, E_{g1}, E_{g2}, e_{g1}, e_{g2}. $\mathbf{E}\cdot\mathbf{r}$ is the dipolar transition operator.

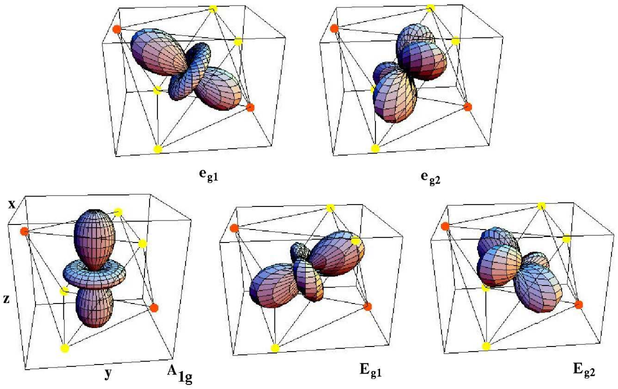

FIG. 5: (Color online) Five BaVS$_3$ V 3d orbitals corresponding to Eq. 1: two e$_g$ (upper panels) and three t$_{2g}$ (lower panels). They are inserted in the orthorhombic phase deformed octahedra, with two inequivalent sulfur atoms, S$_1$ (orange) and S$_2$ (yellow). Axes (x,y,z) correspond to (a,b,c) crystallographic axes in the orthorhombic phase.

The polarization dependent transition probabilities, $P^{\perp}$ for $\mathbf{E}\perp\mathbf{c}$ and $P^{\parallel}$ for $\mathbf{E}\|\mathbf{c}$, are the following:

- Transitions to the higher energy e_g states are not polarization dependent. For both polarizations their probability is $P^{\perp}_{e_g} = P^{\parallel}_{e_g} = 0.4$.
- Transitions to the A_{1g} states are strongly polarization dependent, $P^{\perp}_{A_{1g}} = 0.1$ and $P^{\parallel}_{A_{1g}} = 0.4$.
- Transitions to E_g states are also polarization dependent, $P^{\perp}_{E_g} = 0.5$ and $P^{\parallel}_{E_g} = 0.2$. Thus the total polarization dependent absorption intensity as a function of energy can be written as:

$$
\begin{aligned}
I_{\perp,\parallel}(\epsilon) \propto n_{A_{1g}}(\epsilon)P^{\perp,\parallel}_{A_{1g}} + [n_{E_{g1}}(\epsilon) + n_{E_{g2}}(\epsilon)]P^{\perp,\parallel}_{E_g} \\
+[n_{e_{g1}}(\epsilon) + n_{e_{g2}}(\epsilon)]P^{\perp,\parallel}_{e_g},
\end{aligned}
\tag{3}
$$

where $n_d(\epsilon)$ are unoccupied spectral function weights at a particular final (core-excited) state energy ϵ.

As the transitions to the e_g states are equiprobable for both polarizations, the linear dichroism should be zero for excitations to states with this symmetry. The difference in the transition probabilities to A_{1g} is equal to that of each individual E_g orbital but of opposite sign. Thus an increase in the population of A_{1g} states will tend to reduce the LD or give a negative signal while an increase in the E_g population will tend to increase the LD when defined as $(I_{\perp} - I_{\|})(\epsilon)$.

Summarizing our observations, little difference in the polarization dependence can be detected across the T$_S$ = 240 K hPM to oPM phase transition despite the symmetry break which lifts the degeneracy of the two E_g and two e_g states as shown in Fig. 6 (upper panel). Lowering the temperature below 150 K (oPM-LT) induces an increase in the LD amplitude at 515.8 eV, while the intensity starts to build up at 513.2 eV, where a distinct peak appears below T$_{MI}$ = 69 K. When the temperature is further reduced below the mPI to AFI (T_{χ} = 30 K) phase transition the intensity at 515.8 eV again drops and the 513.2 eV peak intensity strengthens. This could mean that spin ordering has the effect of transfering one part of unoccipied E_g states to lower energy.

The increase in LD amplitude at 513.2 eV and 515.8 eV across the oPM-HT to oPM-LT temperature range might

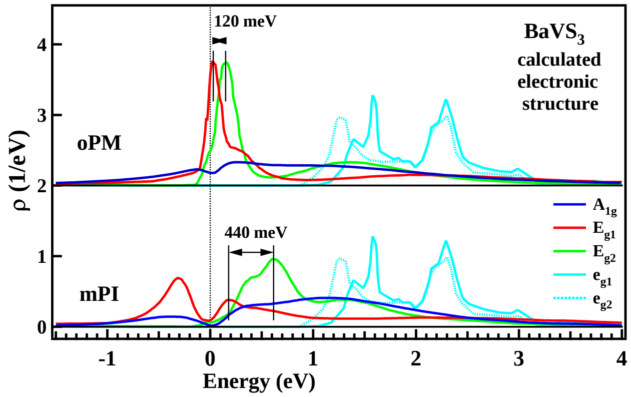

FIG. 6: Local spectral functions from LDA+DMFT calculations of the t_{2g} states in the oPM phase where all V sites are equivalent (upper panel) and mean value of local spectral functions for four inequivalent V-sites for the t_{2g} states in the mPI phase (lower panel). The LDA density of e_g states shown in both panels is the one calculated for the oPM phase, as the calculation for the mPI phase is not available. Fermi level energy is set to 0. LDA and DMFT data have been adapted from the Figs. 2, 7 and 12 of Ref.18.

be interpreted as an increase of the E_g weight in the corresponding small energy range. As the magnetic properties are related to the E_g states, this interpretation is in line with the energy dependence of the ground state magnetic reflection at the (0.226 0.226 0.033) wave vector which shows two V L_3 peaks at similar positions [6]. On the other hand, in the oPM-LT temperature range, there is a formation of CDWs in chains, as shown by pretransitional diffuse lines in x-ray diagrams [3]. It is a dynamical effect, with a typical lifetime of 10^{-12} s [19], which can induce local structure modifications via electron-phonon interaction. As the time scale of XAS is determined by the V L_3 edge core-hole-lifetime of 10^{-15} s, it can probe short-time modifications of unoccupied states related to CDW fluctuations. Similar dynamical local structural change is observed at the Ni K-edge NEXAFS of $PrNiO_3$ [20] system.

Over the oPM-HT temperature range all V sites are equivalent by symmetry, while in the mPI phase there are four inequivalent V-sites in the monoclinic unit cell [21]. Resonant diffraction measurements at the V K edge pointed to the possibility of an orbital ordering of $A0E0$ type (A_{1g}, equal, E_{g1}, equal) accompanying the CDW formation [22]. Collective intersite orbital excitations measured in the dielectric signal support this hypothesis [23]. DMFT calculations confirm that the four inequivalent V-sites have different spectral functions but propose rather an $EE00$ occupation pattern [18]. In terms of *unoccupied* states, two sites have their E_{g2} local spectral function maximum closer to E_F and the other pair have the maximum pushed to higher energy, giving rise to a broad double peak when the mean value for four inequivalent V-sites is presented as in the Fig. 6 (lower panel).

From these considerations we suppose that, below 150 K, the increased LD intensity at 513.2 eV and 515.8 eV is related to the strong high energy transfer of a part of unoccupied E_g states. This shift is itself related to the formation of four inequivalent V-sites which accompanyies CDW formation in the pretransitional fluctuation regime. Possible core-hole effects are difficult to estimate without proper theoretical modeling. It is however reasonable to suppose that difference in core hole interaction across the phases is negligibly small.

V. CONCLUSION

$BaVS_3$ single crystal V L edge x-ray linear dichroism (LD) spectra show changes with temperature. Below 150 K there is a clear LD intensity increase at 513.2 eV and 515.8 eV. Simple symmetry analysis suggests the effect is related to rearrangements in E_g and A_{1g} states. Two V L_3 peaks at similar energies are observed in the energy scan of the ground state (0.226 0.226 0.033) reflection measured by the resonant magnetic x-ray scattering [6]. This confirms that the observed increase of the LD intensity is related to magnetically active E_g states. DMFT calculations [18] predict rearrangements of E_g states in the mPI phase, together with CDW-related formation of four inequivalent vanadium sites with different E_g and A_{1g} spectral functions. Our data show that the E_g rearrangements start at higher temperatures with the formation of CDWs in chains, affecting A_{1g} states. We expect these experimental results to help ongoing efforts to model this complex material as they highlight the need to consider A_{1g} and E_g states as a whole to understand the physical properties of this unusual compound.

Acknowledgments

Fruitful discussions with P. Foury, J.-P. Pouget, S. Tomić, F. Lechermann, S. Barišić, I. Kupčić, M. Grioni, P. Benčok, M.-A. Arrio, P. Sainctavit and Y. Joly are gratefully acknowledged. The work in Lausanne was supported by the Swiss National Science Foundation and its NCCR "MaNEP".

[1] Gardner R, Vlasse M and Wold A 1969 *Acta Crystallogr.* B **25** 781
[2] Mihály G, Kézsmárki I, Zámborszky F, Miljak M, Penc K, Fazekas P, Berger H and Forró L 2000 *Phys. Rev.* B **61** R7831
[3] Fagot S, Foury-Leylekian P, Ravy S, Pouget J-P and Berger H 2003 *Phys. Rev. Lett.* **90** 196401
[4] Inami T, Ohwada K, Kimura H, Watanabe M, Noda Y, Nakamura H, Yamasaki T, Shiga M, Ikeda N and Murakami Y 2002 *Phys. Rev.* B **66** 073108
[5] Nakamura H, Yamasaki T, Giri S, Imai H, Shiga M, Kojima K, Nishi M, Kakurai K and Metoki N 2000 *J. Phys. Soc. J.* **69** 2763
[6] Leininger Ph, Ilakovac V, Joly Y, Schierle E, Weschke E, Bunau O, Berger H, Pouget J-P and Foury-Leylekian P 2011 *Phys. Rev. Lett.* **106** 167203
[7] Mattheiss L 1995 *Solid State Commun.* **93** 791
[8] Whangbo M-H, Koo H-J, Dai D and Villesuzanne A 2002 *J. Solid State Chem.* **165** 345
[9] Lechermann F, Biermann S and Georges A 2005 *Phys. Rev. Lett.* **94** 166402
[10] Nakamura H, Imai H and Shiga M 1997 *Phys. Rev. Lett.* **79** 3779
[11] Kuriyaki H, Berger H, Nishioka S, Kawakami H, Hirakawa K and Lévy F A 1995 *Synth. Met.* **71** 2049
[12] Ilakovac V, Kralj M, Pervan P, Richter M C, Goldoni A, Larciprete R, Petaccia L and Hricovini K 2005 *Phys. Rev.* B **71** 085413
[13] Abbate M, de Groot F M F, Fuggle J C, Ma Y J, Chen C T, Sette F, Fujimori A, Ueda Y and Kosuge K 1991 *Phys. Rev.* B **43** 7263
[14] Park J-H , Tjeng L H, Tanaka A, Allen J W, Chen C T,

Metcalf P, Honig J M, de Groot F M F and Sawatzky G A 2000 *Phys. Rev.* B **61** 11506

[15] Scherz A, Wende H, Baberschke K, Minár J, Benea D and Ebert H 2002 *Phys. Rev.* B **66** 184401

[16] Learmonth T, Glans P A, Guo J H, Greenblatt M and Smith K E 2010 *J. Phys.: Condens. Matter* **22** 025504

[17] Campbell J L and Papp T 2001 *At. Data and Nucl. Data Tables* **77** 1-56

[18] Lechermann F, Biermann S, and Georges A 2007 *Phys. Rev.* B **76** 085101

[19] Pouget J-P, Hennion B, Escribe-Filippini C and Sato M 1991 *Phys. Rev.* B **43** 8421

[20] Acosta-Alejandro M, Mustre de León J, Medarde M, Lacorre Ph, Konder K, and Montano P A, 2008 *Phys. Rev.* B **77** 085107

[21] Fagot S, Foury-Leylekian P, Ravy S, Pouget J P, Anne M, Popov G, Lobanov M V, Greenblatt M 2005 *Sol. St. Sci.* **7** 718

[22] Fagot S, Foury-Leylekian P, Ravy S, Pouget J-P, Lorenzo É., Joly Y, Greenblatt M, Lobanov M V, and Popov G 2006 *Phys. Rev.* B **73** 033102

[23] Ivek T, Vuletić T, Tomić S, Akrap A, Berger H and Forró L 2008 *Phys. Rev.* B **78** 035110